JOURNAL OF MATERIALS SCIENCE 31 (1996) 5709–5715

Chemical vapour growth of HfP whiskers and their properties

S. MOTOJIMA, S. HIRANO
Department of Applied Chemistry, Faculty of Engineering, Gifu University, Gifu 501-11, Japan

M. FUJII
Nagasaki Institute of Applied Science, Nagasaki 851-01, Japan

H. IWANAGA
Faculty of Liberal Arts, Nagasaki University, Nagasaki 852, Japan

Whiskers and ribbon-like single crystals of β-HfP (hexagonal) have been prepared from $HfCl_4 + PCl_3 + H_2 + Ar$ gas mixtures at 1100–1200 °C using a metal impurity-activated chemical vapour deposition process. The growth conditions, morphology and chemical properties were examined. The 3.5–6.5 mm (average 4 mm) long HfP whiskers were obtained at 1200 °C using Si + Pt or Si + Pd mixed impurities. The HfP whiskers were very stable against oxidation up to 3 h exposure at 1000 °C and for 80 min immersion in concentrated HCl solution at 50 °C.

1. Introduction

Much research on transition metal carbides, nitrides, borides or silicides has been carried out during the past decades. However, only a few studies on the transition metal phosphides have been performed, although some transition metal phosphides are of significant interest due to their high thermoelectric power, metallic conduction, as well as good corrosion stability [1, 2].

We have prepared whiskers of TiP [1], ZrP [3], and NbP [4] using metal-activated chemical vapour deposition (CVD), and bulk single crystals of Ni_2P [5], CrP and Cr_3P [6] using vapour-phase phosphidizing of the metals.

The Hf–P system compounds, β-HfP (hexagonal, $P6_3$-*mmc*) [7], α-HfP (cubic), HfP_2 (orthorhombic, P*bnm*) [8], Hf_3P_2 (orthorhombic, P*nma*) [9] and Hf_3P (tetragonal, P42/*n*) [10], were reported. However, the single-crystal growth of the Hf–P compounds, as well as their properties, have never been reported.

In this work, we obtained HfP whiskers and ribbon-like crystals from $HfCl_4 + PCl_3 + H_2 + Ar$ gas mixtures at 1100–1200 °C using the metal impurity-activated CVD process. The growth conditions, morphology, as well as some chemical properties of the Hf-P compound crystals, were examined.

2. Experimental procedure

Fig. 1 shows a schematic drawing of the apparatus used in this work. $HfCl_4$ was prepared by the chlorination of hafnium metal powder by chlorine gas at 800 °C and introduced into the horizontal reaction tube (quartz, 30 mm i.d.) which was heated from the outside. PCl_3 was saturated in a hydrogen carrier gas using a circulation-type saturator and introduced into the reaction zone through an upper gas inlet. A graphite plate ($20 \times 100 \times 0.5\ mm^3$), on which various metal powder impurities were uniformly dispensed, was used as the substrate.

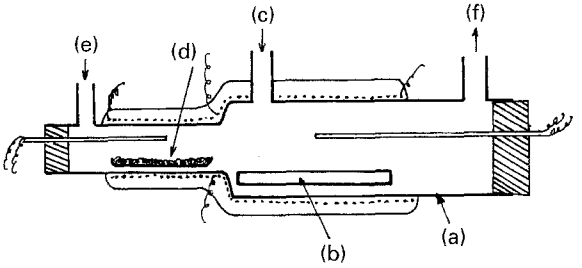

Figure 1 Schematic drawing of the apparatus. (a) Reaction tube (quartz, 30 mm i.d.), (b) substrate (graphite plate, $20 \times 100 \times 0.5\ mm^3$), (c) $PCl_3 + H_2$ gas inlet, (d) hafnium metal powder (average grain size 3 μm), (e) $Cl_2 + Ar$ gas inlet, (f) gas outlet.

3. Results and discussion

3.1. Reaction conditions

It is well known that whisker growth from a vapour phase is generally activated by a metal impurity present on the substrate and one of the most probable growth mechanisms is the vapour–liquid–solid (VLS) mechanism. We have reported that the TiP whisker growth was very activated using the mixed impurities of silicon and transition metals [11]. We used a single metal powder and mixed powder of Si + metal as the

0022–2461

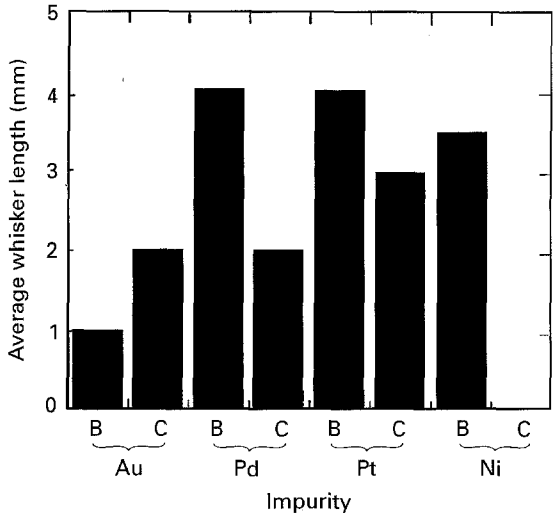

Figure 2 Effect of metal impurities on the average whisker length. Reaction temperature 1200 °C, reaction time 1 h, gas flow ratio (Hf/P) 18, $HfCl_4$ flow rate 18 standard cm^3 min^{-1}. B, graphite substrate on which a mixed powder of Si + metal was deposited; C, graphite substrate on which one kind of metal powder was deposited.

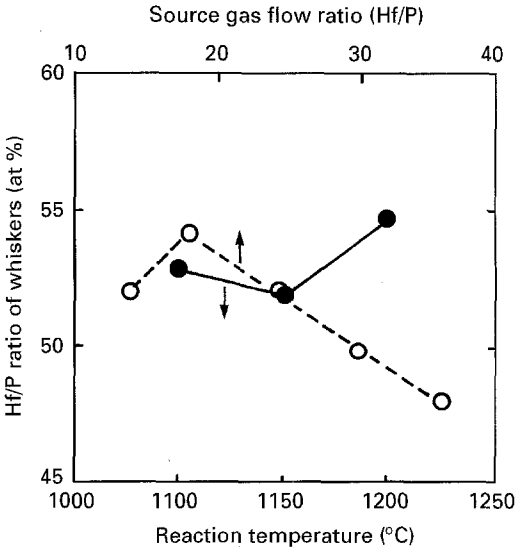

Figure 3 Effect of reaction temperature on the composition (Hf/P) of the whiskers. (○) Reaction temperature 1200 °C. (●) Source gas flow ratio (Hf/P) 18.

impurity. The effect of this type of metal impurity on the whisker growth is shown in Fig. 2, in which reaction temperature, reaction time and gas flow ratio (Hf/P) were fixed at 1200 °C, 1 h and 18, respectively. Using a bare graphite substrate on which metal impurities were not dispensed, only small amounts and short whiskers were deposited. On the other hand, dispensing the mixed impurities of Si + Pd, Si + Pt and Si + Ni on the substrate, large amounts of long thin whiskers or ribbon-like crystals were grown. These whiskers had a length of 3.5–6.5 mm (average 4 mm) at 1200 °C for 1 h reaction time. A single metal powder not mixed with the silicon powder has a weak influence on the thin whisker growth. Subsequently, mixed impurities of Si + Pt were used unless otherwise stated. An appreciable HfP whisker growth was observed above 1100 °C, and the length significantly increased with increasing reaction temperature, reaching 3.5–6.5 mm (average 4 mm) at 1200 °C. The whiskers have a wide range of thicknesses from 2–20 μm irrespective of the reaction temperature and gas flow ratio (Hf/P). The optimum source gas flow ratio (Hf/P) for the thin whisker growth was about 18 and the length significantly decreased above or below this ratio. This may be caused by the lower reactivity of $HfCl_4$ with hydrogen than that of PCl_3.

3.2. Identification of the deposits

The whiskers obtained were identified as β-HfP (hexagonal, $P6_3/mmc$) irrespective of reaction conditions, from the X-ray diffraction pattern and Debye photograph. Fig. 3 shows the effect of reaction temperature and source-gas flow ratio (Hf/P) on the composition of the whiskers obtained using an electron probe microanalyser (EPMA). It was observed that the whiskers generally have a hafnium-rich composition. The homogeneous ranges of the β-HfP were not reported. The deposited phases were only β-HfP, irrespective of the reaction conditions, as already mentioned.

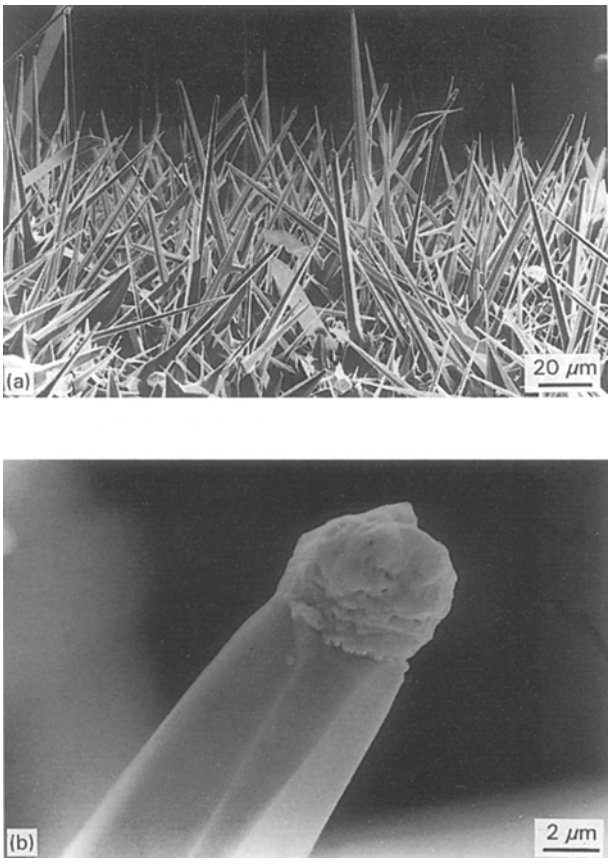

Figure 4 (a) Representative needle-like crystals and (b) an enlarged view of the tip. Reaction temperature 1200 °C; substrate, bare graphite plate on which no metal impurity was deposited.

Accordingly, it may be postulated that β-HfP has wide homogeneous ranges.

3.3. Morphology of the HfP crystals

Fig. 4a shows representative photographs of the needle-like HfP crystals grown on the bare graphite substrate. The needle-like crystals generally have a square cross section, but crystals having a hexagonal

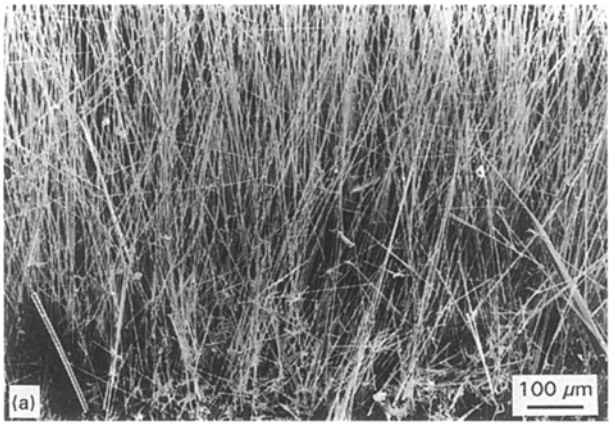

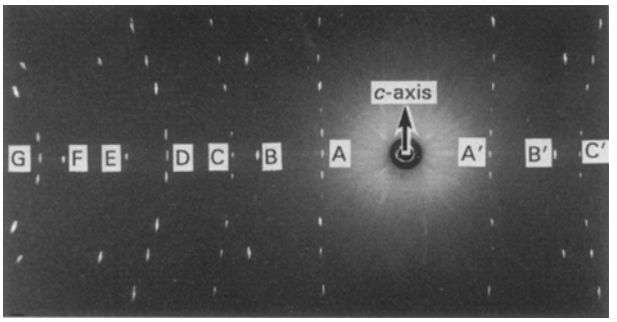

Figure 6 A 90° oscillation X-ray photograph around the growth direction of the thin whisker. Millar indices for β-HfP: A(1 0 $\bar{1}$ 0), A′(0 $\bar{1}$ 1 0), B(1 1 $\bar{2}$ 0), B′(1 $\bar{2}$ 1 0), C(2 0 $\bar{2}$ 0), C′(0 $\bar{2}$ 2 0), D(3 $\bar{1}$ $\bar{2}$ 0), E(3 0 $\bar{3}$ 0), F(2 2 $\bar{4}$ 0), G(3 1 $\bar{4}$ 0).

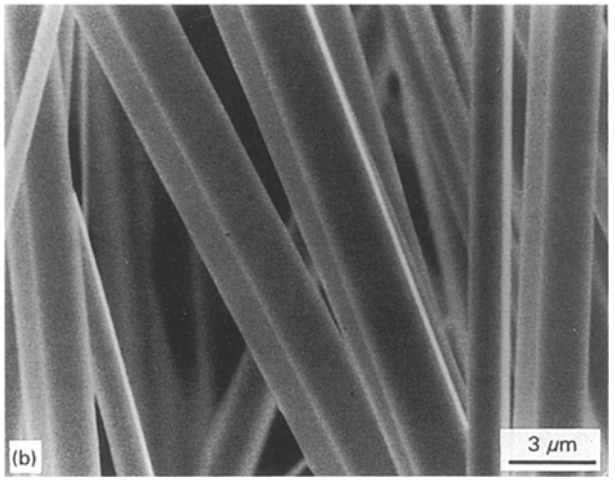

Figure 5 (a) Thin whiskers and (b) an enlarged view. Impurity, Pt + Si; reaction temperature 1100 °C.

cross section were also sometimes observed. An irregular ball-like deposit was always observed on all of the crystal tips, as shown in Fig. 4b. The presence of a small amount of impurities such as iron, cobalt, etc., were observed in the graphite substrate using EPMA. On the other hand, the presence of these impurities was not observed on the tip deposits. However, it may be reasonably considered that a trace amount of impurity metals was included in the tip deposits and accelerated the needle-like crystal growth by the VLS mechanism.

Fig. 5 shows the representative thin whiskers obtained using the mixed impurities of Si + Pt at 1100 °C. The whiskers are generally 1–3 μm thick and have a square cross-section, but whiskers having a hexagonal cross-section were also sometimes observed. Fig. 6 shows the 90° oscillation X-ray photograph around the growth axis of the thin HfP whiskers having a hexagonal cross-section. The (*hki*O) spots of the β-HfP phase are observed on the equatorial line of the photograph. This result suggests that the growth direction of the thin HfP whisker having a hexagonal cross-section is in the *c*-direction. Various types of small needle-like crystals were frequently observed on the tip of the thin whiskers having a square cross-section as shown in Fig. 7. These needle-like crystals

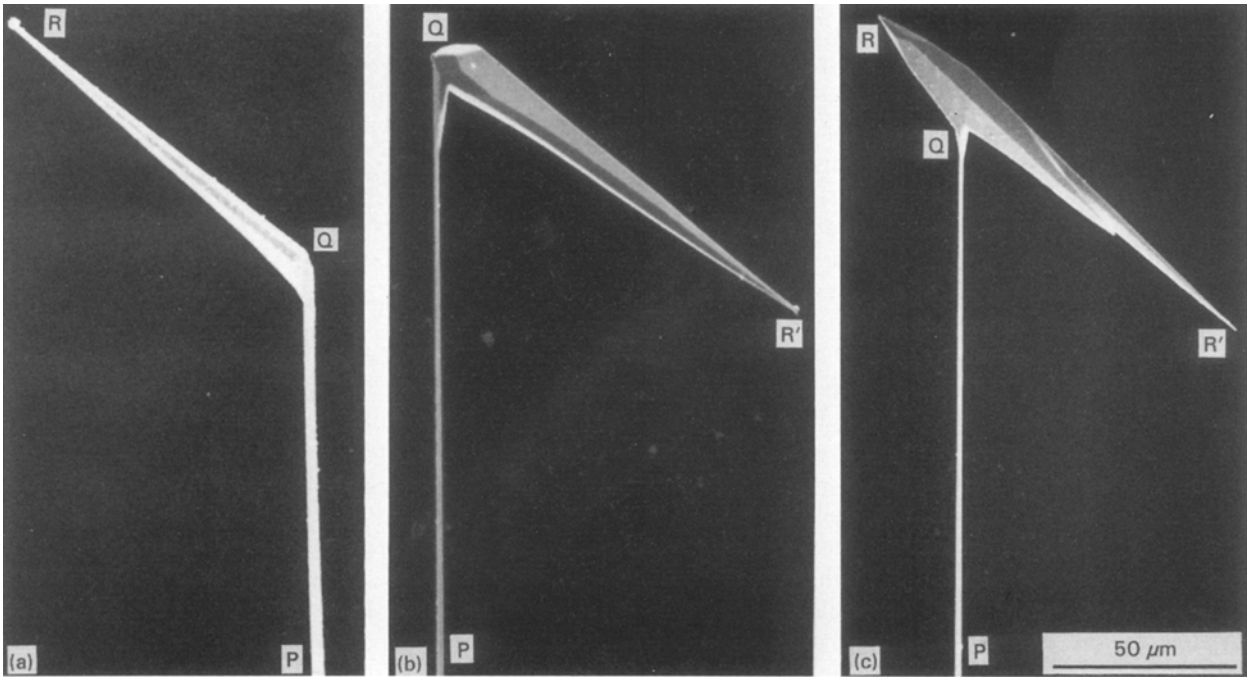

Figure 7 Tip part of the thin whiskers having a square cross-section. Angle between the needle-like crystal tip and the thin whisker: (a) ~ 120°, (b, c) ~ 60°.

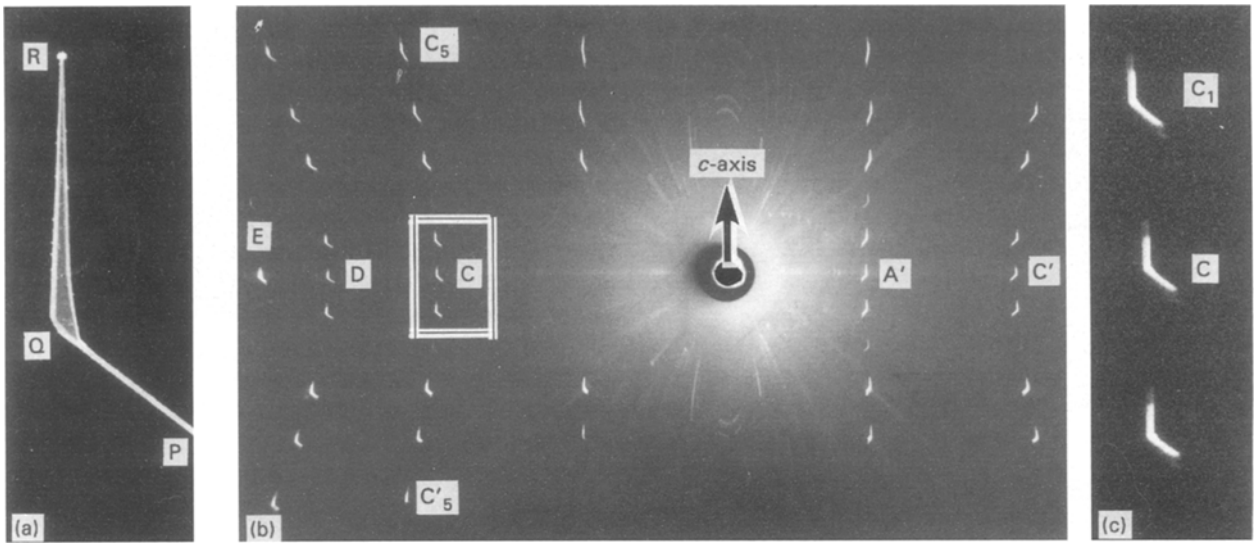

Figure 8 (a) SEM image, (b) 30° oscillation photograph around the growth axis and (c) enlarged photograph of the part outlined by a rectangle in (b). Millar indices for β-HfP: A′(0$\bar{1}$10), C(20$\bar{2}$0), C′(0$\bar{2}$20), C_1(20$\bar{2}$1), C_5(20$\bar{2}$5), D(3$\bar{1}$$\bar{2}$0), E(30$\bar{3}$0).

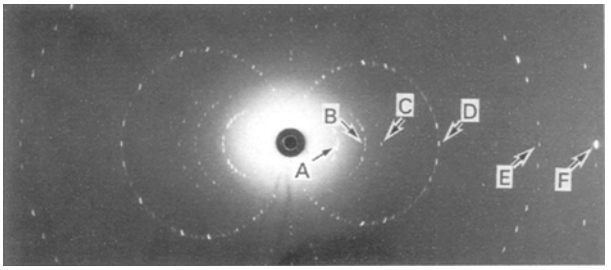

Figure 9 Laue photograph taken from the [1$\bar{1}$00] direction of the QR in Fig. 7c with a cylindrical camera. A(12$\bar{3}$0), B(13$\bar{4}$0), C(14$\bar{5}$0), D(01$\bar{1}$0), E(13$\bar{2}$0), F(12$\bar{1}$0).

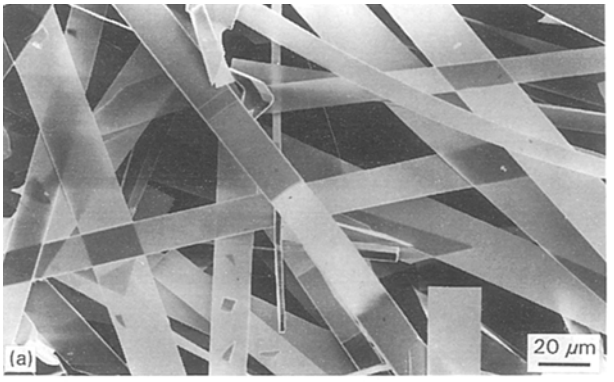

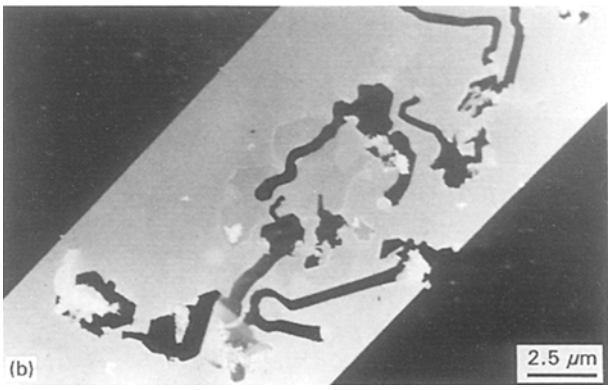

Figure 10 (a) Well-formed ribbon-like crystals and (b) ribbon-like crystals having island depressions.

grew on the whisker tips at about 60° or 120° to the growth axis (PQ in Fig. 7) of the thin whisker. Fig. 8b shows the 30° oscillation photograph around the growth axis (QR) of the needle-like crystals in Fig. 8a. Fig. 8c shows an enlarged photograph of the area "C" outlined by a rectangle in Fig. 8b. All the diffraction spots have the same shape as the tip of the needle-like crystal itself. This result indicates that the needle-like crystal tip (RQ, R′Q or RQR′) and whisker (PQ) is the same single crystal. In the diffraction spots observed on the equatorial line, no spots (A, B and C) as shown in Fig. 6 are contained, because of the 30° oscillation photograph. The lattice parameter, *c*, was estimated to be 1.239 nm using a separation value for C_5–C'_5 of 55.6 mm and a camera radius of 35.0 mm. This value is in good agreement with the reported value of 12.37 nm [12]. Accordingly, the growth axis of the needle-like crystal tip (QR direction) is parallel to the *c*-axis. Fig. 9 shows the Laue photograph taken with the incident X-ray beam parallel to the lateral face of the needle-like crystal with a hexagonal cross-section, by a cylindrical camera. This photograph shows that the lateral face of the needle-like crystal is (11$\bar{2}$0). On the other hand, the growth axis of the whisker (PQ) is considered to be in the direction rotated by about 60° or 120° from the *c*-axis around the *a*-axis.

Using Si + Pt mixed impurities, well-formed ribbon-like single crystals, as well as thin whiskers, were obtained. The representative well-formed, ribbon-like crystals obtained at 1100 °C are shown in Fig. 10. The ribbon-like crystals generally have a smooth surface with a 10–20 μm width and are very thin. However, some crystals have island-like patterns, and are extremely thin or apparently transparent as shown in Fig. 10b. Fig. 11 shows various types of deposits observed on the surface of the ribbon-like crystals. Hexagonal pyramidal crystals having many distinct

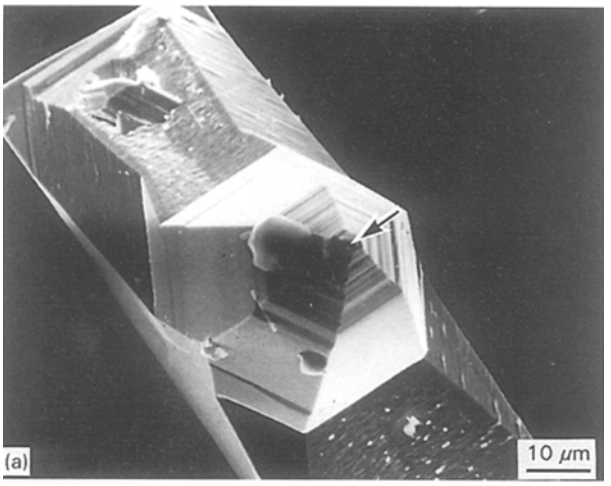

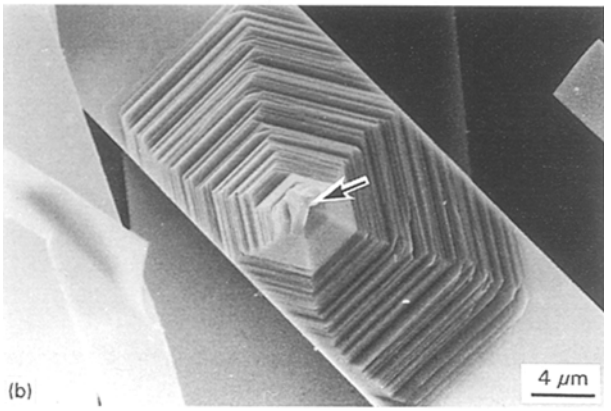

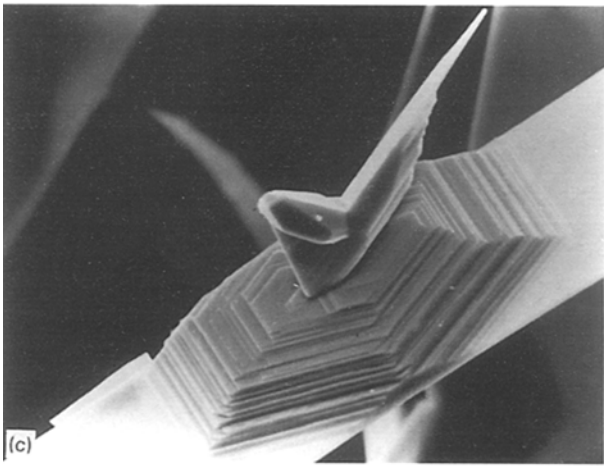

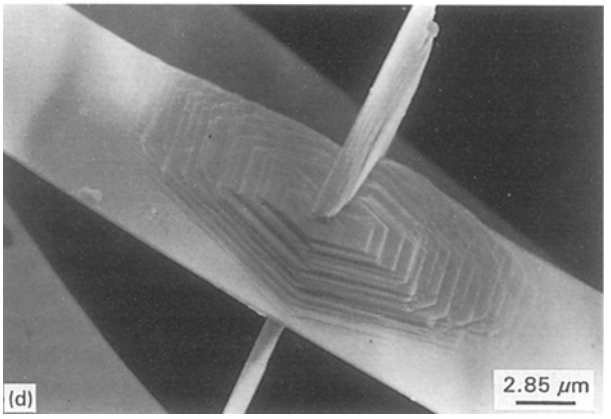

Figure 11 Hexagonal growth steps observed on ribbon-like crystals. (a, b) Hexagonal pyramidal crystal, (c) hexagonal pedestal-like crystal, (d) hexagonal crystal through which a pillar crystal grew.

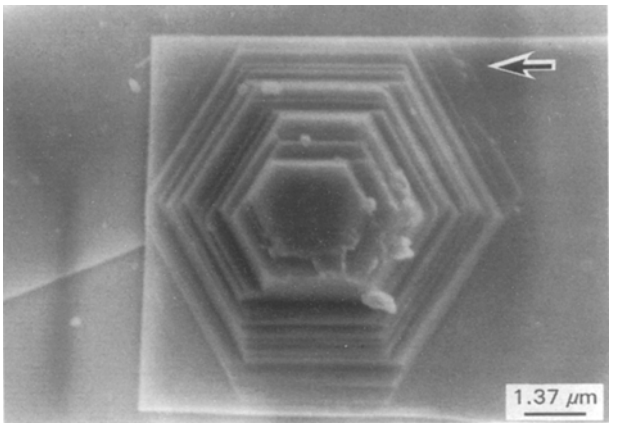

Figure 12 Hexagonal growth steps deposited on the surface of ribbon-like crystals. An arrow indicates the growth direction of the ribbon-like crystal.

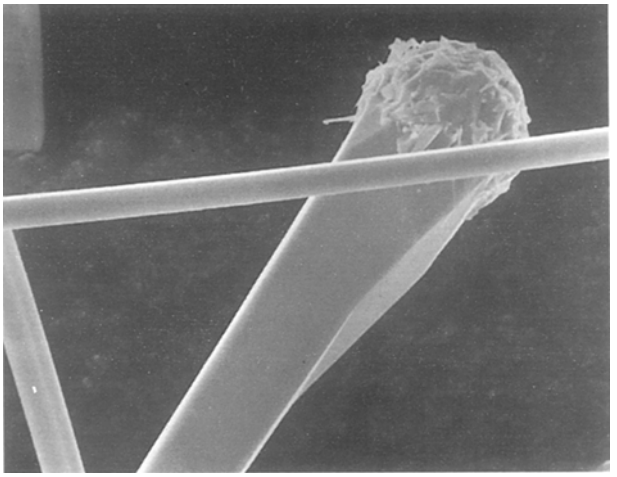

Figure 13 The tip of a ribbon-like crystal.

growth steps were sometimes observed, as seen in Fig. 11a and 11b. Furthermore, some small deposits were also observed on the tip of the pyramidal crystals (arrow). Fig. 11c shows the well-formed, bird-like crystals grown from these tip deposits. The presence of impurity metals was not observed in these tip deposits by EPMA. The lowest eutectic temperatures of the Hf–P–Pt, Hf–P–Si, or Hf–P–Pt–Si are not known. However, it may be considered that the growth of these hexagonal deposits is activated by the metal impurities present on the surface of the ribbon-like crystals. Fig. 11d shows another type of hexagonal deposit through the central part of which a pillar crystal vertically grew. The direction of an edge of the hexagonal deposits was generally 30° from the growth direction of the ribbon-like crystals. This morphology suggests that the growth direction of this ribbon-like crystal will be $[1\,0\,\bar{1}\,0]$. On the other hand, the growth direction of the ribbon-like crystal as shown in Fig. 12 is parallel to the direction of an edge of the hexagonal deposit. These crystals, growth in the $[1\,1\,\bar{2}\,0]$, were rare. The ribbon-like crystals could not be obtained without the presence of the mixed impurity of Si + Pt. Fig. 13 shows the tip of the ribbon-like crystals; irregularly shaped deposits were observed on the tip. The

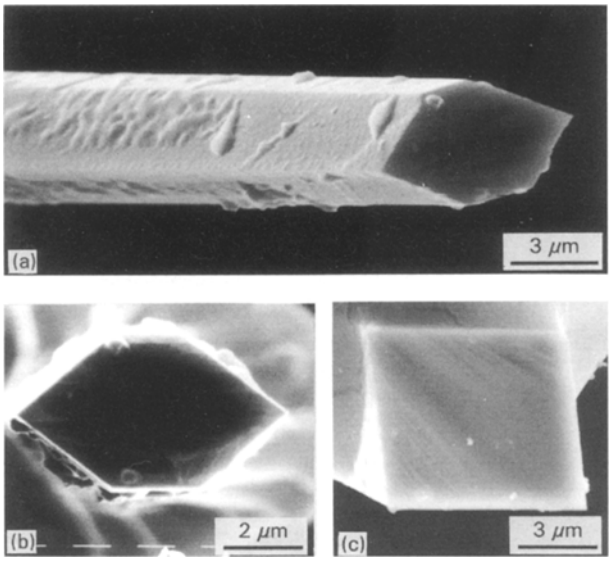

Figure 14 Ruptured cross-section of a whisker. (a) Ruptured cross-section of a whisker having a deformed hexagonal cross-section which was sometimes observed. (b) Horizontal cross-section of (a) in which the photograph was taken from the axis direction of the whisker, (c) horizontal cross-section of the whiskers having a square cross-section which were commonly observed.

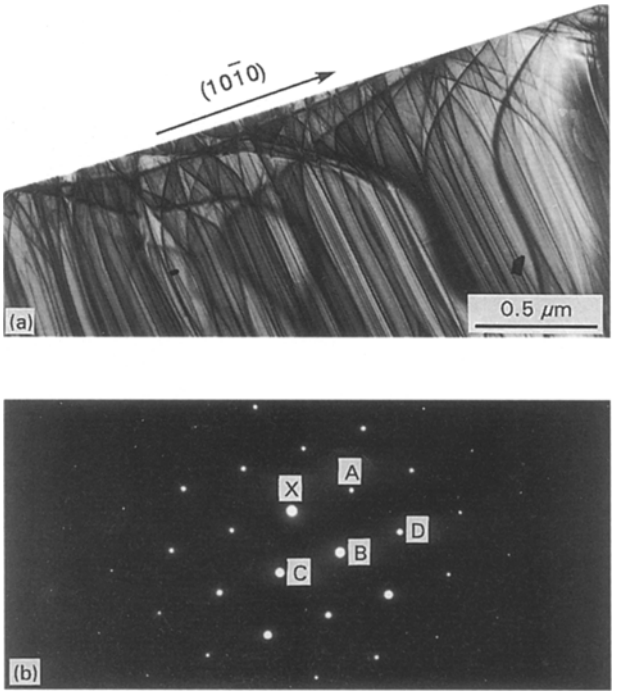

Figure 15 (a) Dark-field image of a ribbon-like crystal and (b) the electron diffraction patterns of the crystal X(0 0 0 0), A(1 0 $\bar{1}$ 0), B(0 1 $\bar{1}$ 0), C($\bar{1}$ 1 0 0), D(1 1 $\bar{2}$ 0).

presence of the platinum and/or silicon impurity used was not observed on the tip by EPMA. However, it may be postulated that the growth of the ribbon-like crystals is also closely related to the VLS mechanism activated by metal impurities.

Fig. 14a shows the fractured cross-section of a whisker having a deformed hexagonal cross-section which was sometimes observed. Fig. 14b shows the vertical view in which the photograph was taken from the axial direction of the whisker. It can be seen that the cross-section is not a regular hexagonal but deformed hexagonal constructed by inner angles of about 80° and 140°. Fig. 14c shows that in the fractured cross-section, whiskers with a square cross-section were commonly observed. It can be seen that the cross-section is not a regular square but rather a somewhat deformed square having about 85° and 95° inner angles. The whiskers shown in Fig. 7 are also of this type.

Fig. 15 shows part of the ribbon-like crystal and the electron diffraction pattern of this crystal. From this pattern, it can be seen that the crystal face of the ribbon-like crystals is the *c*-face and the growth direction is [1 0 $\bar{1}$ 0]. Striation patterns observed in Fig. 15a are considered to be fault planes parallel to the (1 0 $\bar{1}$ 0) plane.

Fig. 16 shows a dark-field image of a whisker and the electron diffraction patterns. From this diffraction pattern, it can be seen that this whisker grew to the direction rotated by about 60° from the *c*-axis around the *a*-axis. Accordingly, this whisker is considered to be the same type as the whisker (PQ) shown in Fig. 7. Fig. 17 shows a dark-field image of another type of whisker and the electron diffraction patterns. It can be seen that this whisker has many faults formed in the vertical direction of the whisker axis, and the growth direction is [1 0 $\bar{1}$ 2].

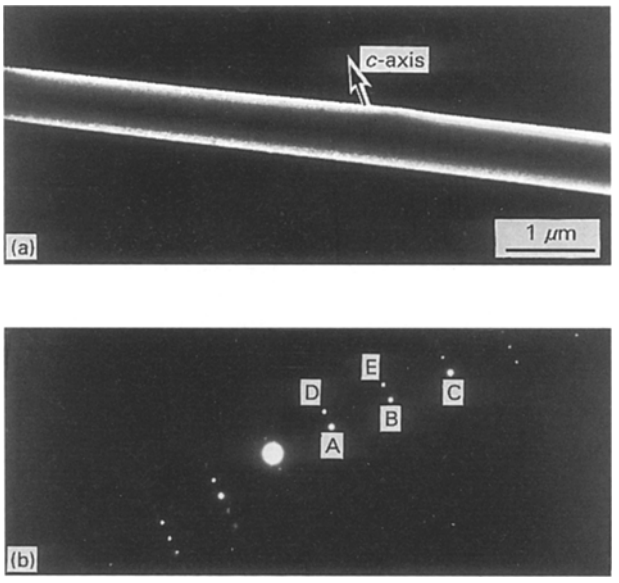

Figure 16 (a) Dark-field image of a whisker having many faults and (b) the electron diffraction patterns. A(1 2 $\bar{3}$ 0), B(2 4 $\bar{6}$ 0), C(3 6 $\bar{9}$ 0), D(1 2 $\bar{3}$ 1), E(2 4 $\bar{6}$ 1).

3.4. Chemical properties

The pulverized HfP whiskers were rapidly heated to 1000 °C using an infrared concentrated gold image furnace under an air flow of 60 standard cm^3 min^{-1} which was maintained for 3 h. However, no weight change, surface roughening or pulverizing of the sample was observed after this 3 h exposure. This result suggests that the HfP whiskers have a high oxidation resistivity up to 1000 °C in air.

The mirror-like highly polished cross-sections of the HfP crystals were immersed in a concentrated HCl solution maintained at 50 °C for 40–80 min. No

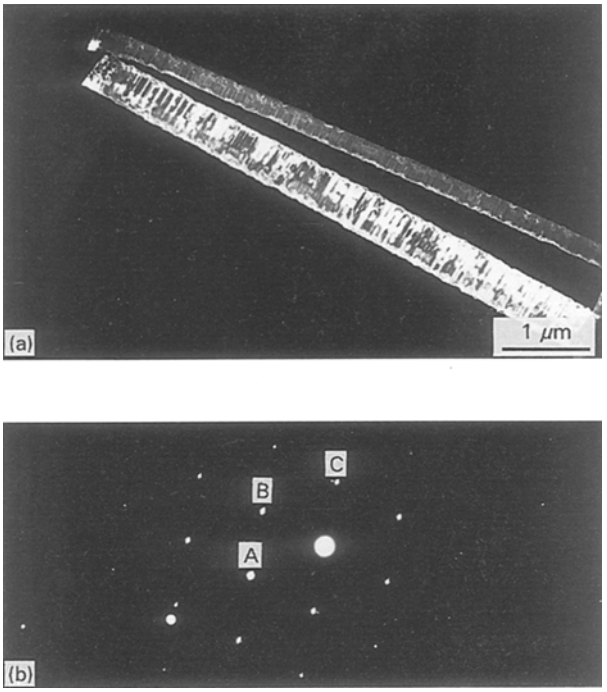

Figure 17 (a) Dark-field image of a whisker having many faults and (b) the electron diffraction patterns. A(0 1 $\bar{1}$ 0), B(1 0 $\bar{1}$ 2), C(1 $\bar{1}$ 0 2).

etching or roughening of the mirror face was observed after a 40 min immersion, while some etching patterns were observed after 80 min. That is, the HfP whiskers were very stable in concentrated HCl solution. It was observed that the order of corrosion stability in concentrated HCl of the group IV elements was as follows: HfP > ZrP > TiP.

4. Conclusion

Whiskers and ribbon-like crystals of β-HfP have been prepared from $HfCl_4 + PCl_3 + H_2 + Ar$ gas mixtures at 1100–1200 °C using a metal-impurity activated CVD process. The growth conditions, morphology and some properties were examined. The 3.5–6.6 mm (average 4 mm) long HfP whiskers were obtained at 1200 °C using mixed metal powder impurities of Si + Pt and Si + Pd. The growth direction of the thin whiskers having a hexagonal cross-section, was in the *c*-axis. On the other hand, two kinds of growth direction of the whiskers having a square cross-section (rotated by about 60° from the *c*-axis around the *a*-axis, and the [1 0 $\bar{1}$ 2] direction) were observed. The crystal face of the ribbon-like crystals was the *c*-face and the growth direction was [1 0 $\bar{1}$ 0]. The HfP whiskers were very stable against oxidation at 1000 °C and in concentrated HCl solution at 50 °C.

References

1. S. MOTOJIMA, T. WAKAMATSU and K. SUGIYAMA, *J. Less-Common Metals* **82** (1981) 379.
2. S. MOTOJIMA, T. WAKAMATSU, Y. TAKAHASHI and K. SUGIYAMA, *J. Electrochem. Soc.* **123** (1976) 290.
3. S. MOTOJIMA, Y. TAKAHASHI and K. SUGIYAMA, *J. Crystal Growth* **30** (1975) 1.
4. S. MOTOJIMA, T. IZUSHI, K. SUGIYAMA and Y. TAKAHASHI, *Bull. Chem. Soc. Jpn* **49** (1976) 2122.
5. S. MOTOJIMA, M. NAITO and M. HAYASHI, *J. Crystal Growth* **73** (1985) 111.
6. S. MOTOJIMA and T. HIGASHI, *ibid.* **73** (1985) 639.
7. W. JEITSCHKO and H. NOWOTNY, *Monatsh. Chem.* **93** (1962) 1107.
8. F. FULLIGER, *Nature* **204** (1964) 775.
9. T. LUNDSTROM, *Acta. Chem. Scand.* **22** (1968) 2191.
10. V. PATHANASIN, S. THANOMKUL and S. PREMATUS, *Acta. Crystallogr. Sec. C* **39** (1983) 683.
11. S. MOTOJIMA, I. HASEGAWA, K. KUROSAWA, S. HIRANO and H. IWANAGA, *Mater. Lett.*, **22** (1995) 255.
12. JCPD No. 15–730 (Joint Committee on Powder Diffraction Swathmore, PA).

Received 17 February
and accepted 1 December 1995